

Inorganic Chemistry Communications

journal homepage: www.elsevier.com/locate/inoche



Short communication

Comparative excited state dynamics of metallo *meso*-(4-fluoro-2,6-dimethylphenyl) porphyrins

William Crisp,† Stephon Amadis Fagan-Avery,† Brandon M. Campbell, Daniel R. Morphet, Kristopher G. Reynolds, Bryan Kudisch, Miguel I. Gonzalez, Shao-Liang Zheng, Dilek K. Dogutan* and Daniel G. Nocera*

Department of Chemistry and Chemical Biology, Harvard University, Cambridge, MA 02138, USA

ARTICLE INFO

Keywords: Manganese and palladium porphyrins Excited state dynamics Picosecond decay Laser spectroscopy

ABSTRACT

The Mn(III)Cl and Pd(II) meso-(4-fluoro-2,6-dimethyl-phenyl) porphyrins have been synthesized and structurally characterized by x-ray crystallography. Together with its Zn(II) congener, this homologous series of porphyrins show the manifestation of d-d states and spin-orbit coupling on the excited state dynamics of metalloporphyrins.

1. Introduction

The electronic structure of porphyrins is described by the Gouterman "four-orbital" model [1-3] derived from the π - π * transitions, common to the frontier molecular orbitals of cyclic π -aromatics. The HOMOs are of a_{1u} and a_{2u} symmetries and the LUMOs are a degenerate set of eg orbitals. The electronic spectra therefore arise from a ¹A_{1g} ground state to ¹E_u excited states, thus accounting for the Soret and Q bands in porphyrin absorption spectra. These states also dominate the excited state properties of porphyrins when they coordinate closedshell metals. When coordinating open-shell metals, lowlying d-d states, of high multiplet may intervene and dramatically perturb the excited state dynamics. In this study, we focus on a homologous series of metalloporphyrins functionalized at the meso position with the electron-withdrawing 4-fluoro-2,6-dimethylphenyl 5,10,15,20-tetrakis(4-fluoro-2,6-dimethylphenyl) porphyrin (TFP) has been functionalized with the open-shell Mn(III) and closed-shell Pd(II). These porphyrins have been structurally characterized by single-crystal X-ray crystallography. Femtosecond transient absorption spectroscopy reveals that the Mn(III)TFP(Cl) has a sub-ps singlet excited state lifetime that is much shorter than that of Pd(II)TFP, whose lifetime is in the picosecond time regime despite the absence of low-lying d-d states. Though longer than Mn(III)TFP(Cl), the singlet excited state lifetime of Pd(II)TFP is much shorter than its closed-shell congener Zn(II)TFP, which possess a singlet excited state lifetime of 2.4 ns. The 10^3 -fold difference in singlet lifetime between Pd(II) and Zn(II) TFP systems is indicative of the role that spin-orbit coupling plays in promoting intersystem crossing from the π^* excited state in closed-shell porphyrin systems.

2. Experimental

2.1. Materials and methods

Unless otherwise noted, chemicals were obtained from commercial suppliers at the highest purity available and used without further purification. Free base TFP could be synthesized at high yields under modified synthetic protocols [4]. Specifically, Lindsey high dilution porphyrin formation reaction [5], when performed in a nitrogen filled glovebox atmosphere, leads to the formation of porphyrinogen in high yields; the porphyrinogen is the only major product obtained based on the TLC analyses. Additionally, the subsequent chemical oxidation step proceeds in higher yields. Accordingly, the TFP is isolated in higher quantities $(\sim 60 \text{ mg})$ vs standard conditions $(\sim 25 \text{ mg})$. Due to these improvements in the synthesis using TFP as an exemplar, this porphyrin was chosen for photophysical studies. ¹H and ¹⁹F NMR spectra (Figures S1-S6) were recorded at the Harvard University Department of Chemistry and Chemical Biology's Laukien-Purcell Instrumentation Center on a JEOL ECZ400S spectrometer operating at 400 MHz. Absorption spectra were taken with a 1.0 cm quartz cuvette on an Agilent

^{*} Corresponding authors at: Department of Chemistry and Chemical Biology, Harvard University, Cambridge, MA, 02138, United States of America. E-mail address: dkiper@fas.harvard.edu and dnocera@fas.harvard.edu.

Cary 5000 UV-Vis-NIR spectrophotometer. Mass spectrometry (Figures S7–S9) was performed at the Harvard Center for Mass Spectrometry.

2.2. Synthesis of metallo-5,10,15,20-tetrakis(4-fluoro-2,6-dimethylphenyl) porphyrins

Pd(II)TFP. Freebase TFP (57.0 mg, 0.071 mmol) and Pd(OAc)₂ (400 mg, 1.78 mmol, 25.0 equiv.) were dissolved in HOAc (20 mL). The resulting solution was heated at reflux for 48 h and then cooled to room temperature. The reaction mixture was concentrated to dryness in vacuo before being redissolved in CH2Cl2 (200 mL) and treated with TEA (1 mL). The organic phase was washed with deionized water (200 mL), brine (200 mL), and dried over MgSO₄. The resulting solution was concentrated to dryness in vacuo before being redissolved in minimal hexane:CH2Cl2 (~4 mL, 3:1). Column chromatography (silica, hexane:CH2Cl2 (3:1)) afforded the product as a light-orange liquid that was concentrated to dryness yielding a bright orange powder. (12 mg, 19% isolated yield). ¹H NMR (400 MHz, CD_2Cl_2) δ (ppm): 8.60 (s, 8H), 7.20 (d, J = 8 Hz, 8H), 1.85 (s, 24H). ¹⁹F NMR (400 MHz, CD_2Cl_2) $\delta(ppm)$: –116.11. HRMS $[M = C_{52}H_{40}F_4N_4Pd]$ (m/z): calcd (obsd), 902.2218 (902.2233). λ_{abs} (CH₂Cl₂) 415, 523, 566 nm.

Mn(III)TFP(Cl). Freebase TFP was used as received from Frontier Scientific (40 mg, 0.05 mmol) and Mn(OAc)₂ (87 mg, 0.5 mmol, 10 equiv.) was dissolved in DMF (15 mL). The resulting solution was heated at reflux under nitrogen for 48 h and then cooled to room temperature. The reaction mixture was concentrated to dryness in vacuo before being redissolved in CH2Cl2 (200 mL) and treated with TEA (1 mL). The organic phase was washed with deionized water (200 mL) and brine (200 mL), then dried over MgSO₄. The solution was again concentrated to dryness in vacuo before being redissolved in minimal ethyl acetate:CH2Cl2 (~4 mL, 3:1). Biotage automated column chromatography [silica, ethyl acetate: CH₂Cl₂ (3:1)) afforded the product as a dark green liquid that was concentrated to dryness forming a dark-green powder. (42 mg, quantitative isolated yield) ¹⁹F NMR (400 MHz, CD₂Cl₂): δ(ppm) – 115.11. ESI-MS $[M = C_{52}H_{40}F_4N_4Mn]$ (m/z): calcd (obsd), 851.2564 (851.2549). λ_{abs} (CH₂Cl₂) 373, 400, 478, 533, 585, 620 nm.

2.3. X-ray Crystallographic Methods

Red crystals of Pd(II)TFP and Mn(III)TFP(Cl) suitable for single-crystal X-ray diffraction were obtained by vapor diffusion technique using hexanes (anti-solvent) and THF (solvent). Solutions (1 mL) of Pd(II)TFP (10 mg) and Mn(III)TFP(Cl) (10 mg) in THF were prepared in small scintillation vials (10 mL). These vials were then placed in the larger scintillation vials (20 mL) containing hexanes (1 mL). Red crystals of Pd(II)TFP

were obtained at 4 °C in a week. We did not observe crystal formation for $Mn(III)TFP^+$ so the sample was moved into a glove box freezer kept at -34 °C. Dark blue-green crystals of Mn(III)TFP(CI) suitable for single-crystal X-ray diffraction were obtained within a week of crystallization.

X-ray diffraction analysis of Pd(II)TFP•THF (Figure S10) was performed on a single-crystal coated with Paratone-N oil and mounted on a glass fibers. During the experiments, crystals were frozen at 100 K using an Oxford Cryosystems Cryostream. Data were collected at ChemMatCARS at the Advanced Photon Source at Argonne National Laboratory using synchrotron radiation ($\lambda = 0.41328 \text{ Å}$) on a Huber three-circle diffractometer equipped with a Pilatus 1M(CdTe) detector. The crystal was found to be a four-component non-merohedric twin based on the diffraction pattern. The program CELL_NOW was used to determine the orientation matrices [6]. The second, third, and fourth domains were found to be related to the first domain by 180° (second domain) and 90° (third and fourth domains) rotations around the real axis [1 0 0]. Raw data for all four components were integrated and corrected for Lorentz and polarization effects using Bruker AXS SAINT software and corrected for absorption using TWINABS [7,8].

The structure for Mn(III)TFP(Cl)(THF)•1.5THF (Figure S11) was collected on a Bruker three-circle platform goniometer and an Oxford cryostream cooling device operating at 100 K. Radiation was from a Cu Ka (λ = 1.54178 Å) source on a Bruker SMART APEX II diffractometer. Crystal was mounted on a cryoloop using Immersion oil – NVH type. Data was collected as a series of φ and ω scans at –30°, –55°, –80°, 30°, 55°, 80° and 115° in 2 θ . Data were integrated using Bruker AXS SAINT software [7] and scaled with multi-scan absorption correction using SADABS [9]. Space group assignments for both structures were determined by examination of systematic absences, E-statistics, and successive refinement of the structures.

Both structures were solved by intrinsic phasing using SHELXT and refined using SHELXL operated in the OLEX2 interface [10-12]. The program PLATON was employed to confirm the absence of higher symmetry space groups [13]. Thermal parameters were refined anisotropically for all non-hydrogen atoms. Hydrogen atoms were placed in ideal positions and refined using a riding model. Outlier reflections were omitted from refinement when appropriate. For Pd(TFP)•THF, disorder of the tetrahydrofuran solvent molecule required a combination of displacement parameter restraints (SIMU and RIGU) and distance restraints (DFIX). A portion of the structure contains electron density that could not be modeled. This electron density is attributed to severely disordered solvent molecules that occupy spaces between the porphyrin complexes. Consequently, the unassigned electron density was accounted for using the program SQUEEZE as implemented in the PLATON interface [14]. For Mn(III)TFP(Cl)(THF)•1.5THF, severe disorder of the Mn complex required restraints on bond lengths and constraints of the atomic displacement parameters on each pair of disorder fragments (SADI, SAME and EADP), as well as the restraints of the atomic displacement parameters (SIMU and RIGU) [15]. Additional crystallographic data are provided in Table S1 and in the crystallographic information file, and atomic displacement parameter plots are shown in Figs. S9 and S10

2.4. Time-Resolved Spectroscopy

The data were acquired using a single-shot probereferenced broadband transient absorption (TA) setup, the design of which was reported previously [16]. Briefly, a Ti:Sapphire regenerative amplifier (Coherent Libra-HE) provides 3 W fundamental pulses (800 nm, 50 fs) at a frequency of 1 kHz. The 400 nm pump pulses were generated by seeding an OPerA SOLO (Coherent) with 2 W of the fundamental output of the amplifier. Another fraction (~1 mW) of the fundamental was aligned onto a 1.7 m computer-controlled, motorized translation stage (Aerotech ATS62150, controller) equipped with a hollow retro-reflector, which furnished the pump-probe delay times used in the TA experiments. After the translation stage, the beam was focused with a 100 mm focal length lens onto a 2 mm calcium fluoride (CaF2) crystal to generate a chirped white light continuum. To avoid thermal damage, the crystal was continuously translated backand-forth perpendicular to the input beam. The resulting white light pulses were reflectively collimated and aligned onto a 15 mm translation stage (PhysikInstrumente, M-111.DG. Mercury controller). A notch filter removed the residual 800 nm fundamental from the white light continuum and was subsequently sent onto a broadband reflective neutral density filter to generate probe (reflected) and reference (transmitted) pulses of approximately equal intensity. Subsequently, pump, probe, and reference pulses were reflectively focused into the sample (f = 200mm). After passing through the sample, both transmitted probe and reference pulses were reflectively collimated prior to being sent into a fused silica prism (OptoSigma, DPSQ-20-10H) spectrograph (f = 250 mm) equipped with two 16-bit, 512 pixel chargecoupled devices (Hamamatsu S7030-0906). Data acquisition was enabled by a custom-built interface board from Entwicklungsbüro Stresing. Differential normalized transmittance signals were collected on a shot-to-shot basis with the pump chopped at 500 Hz. One transient absorption trace consisted of 200 probe shots resulting in 100 differential spectra which were averaged at each timepoint. Data presented in this study

Ar
$$\frac{\text{Pd}(\text{OAc})_2}{\text{HOAc}}$$

Ar $\frac{\text{HOAc}}{\text{reflux}, 48 \text{ h}}$

Ar $\frac{\text{Mn}(\text{OAc})_2}{\text{DMF}}$

Ar $\frac{\text{Mn}(\text{OAc})_2}{\text{reflux}, 48 \text{ h}}$

Ar $\frac{\text{Mn}(\text{OAc})_2}{\text{Pomp}}$

Ar $\frac{\text{Mn}(\text{OAc})_2}{\text{Pomp}}$

Scheme 1. Synthesis of two Pd(II)TFP and Mn(III)TFP(Cl). The Mn(III)Cl was isolated from work-up with ethyl:acetate: CH_2Cl_2 (3:1) solvent mixture.

was obtained by recording 15 transient absorption traces and averaging the results. Time constants were calculated by fitting the kinetic data in both Surface Xplorer (Ultrafast Systems) and IgorPro (Wavemetrics) with the appropriate single or double exponential fit functions that minimize the fit residuals for each best fit.

3. Results and discussion

3.1. Synthesis and structural chemistry

The synthetic schemes for the metal insertion of Pd(II) and Mn(III) into freebase TFP is shown in Scheme 1. Metalation of the free base TFP with Pd(II) was performed at reflux with Pd(OAc)₂ dissolved in HOAc. The Mn(III) metalation was performed in reflux with Mn(OAc)₂ dissolved in DMF. Pd(II)TFP was purified with flash column chromatography using silica as the stationary phase and hexane:CH₂Cl₂ (3:1) as the mobile phase. Mn(III)TFP, however, was purified using a solvent mixture of ethyl acetate: CH2Cl2 (3:1) on a Biotage automated flash column chromatography instrument. The Mn(III)TFP+ compound was isolated with an axial chloride, likely furnished from the mobile phase during column chromatography work-up and the THF apical ligand resulted from the crystal growing process. Pd(II)TFP and Mn(III)TFP(Cl) porphyrins were characterized by ¹H (Figures S1-S3, S5 and S6), ¹⁹F (Figures S4, S6) NMR, and MALDI-TOF and ESI-MS (Figures S7, S8). ESI-MS data revealed only the presence of Mn(II)TFP without the Cl and THF apical ligands due to cleavage of the apical ligands from the high-voltage ionization of the mass spectrometry technique.

Pd(II) and Mn(III)Cl TFP compounds were characterized by single-crystal X-ray diffraction (Table S1). The structure of Pd(II)TFP confirmed formation of a square planar Pd(II) complex of the TFP ligand (Figure 1). The Pd(II) center resides on a crystallographic inversion center, resulting in two sets of symmetry-equivalent Pd-N bond distances (2.01389(8) Å and

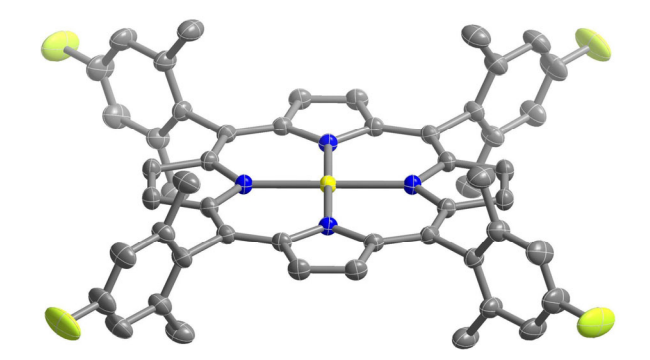


Fig. 1. Crystal structure of Pd(II)TFP. Yellow, yellow green, red, blue, and grey ellipsoids represent Pd, F, O, N, and C atoms, respectively. Hydrogen atoms are omitted for clarity.

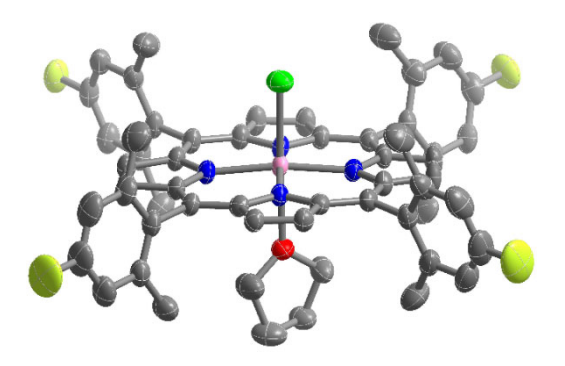


Fig. 2. Crystal structure of Mn(III)TFP(Cl)(THF). Pink, yellow green, red, blue, green, and grey ellipsoids represent Mn, F, O, N, Cl and C atoms, respectively. Hydrogen atoms have been omitted for clarity.

2.01477 Å) and N-Pd-N bond angles (90.054(3)° and 89.946(3)°). These bond metrics correspond well with the average Pd-N distance (2.02(2) Å) and N-Pd-N angle (89.9(9)°) of Pd(II) porphyrin complexes reported in the Cambridge Structural Database [17]. Tetrahydrofuran solvent molecules were located above and below the plane of the Pd complex (Figure S10). The closest distance between the THF molecules and the Pd center was found to be greater than 3 Å, indicating no significant interactions between THF and the Pd center. For the case of Mn(III)TFP(Cl), in addition to the axial chloride, a THF from the crystallization solvent mixture completes the six-coordinate ligand field (Figure S11). Severe disorder in the structure arising from cocrystallized THF solvent precluded accurate determination of bond distances and angles. However, the formation of a pseudo-octahedral Mn porphyrin complex with Cl- and THF at the axial sites is clearly distinguished (Figure 2).

3.2. Electronic spectroscopy

The UV-vis spectra of Pd(II)TFP and Mn(III)TFP(CI) are shown in Figure 3. The absorption spectra of both metalloporphyrins are dominated by the Soret and Q

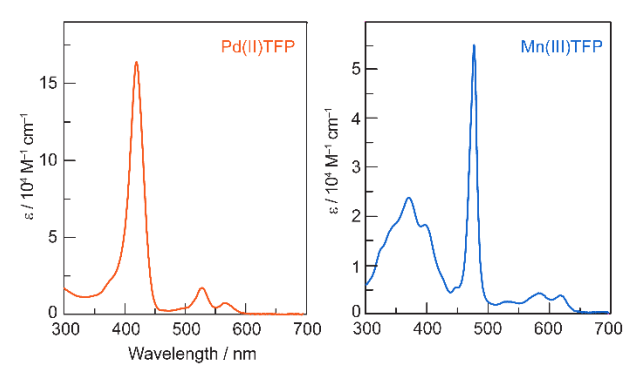


Fig. 3. Absorption spectrum of Pd(II)TFP and Mn(III)TFP(CI) in CH_2CI_2 at room temperature.

band absorption profiles. The D_{4h} symmetry of Pd(II)TFP and C_{4v} symmetry of Mn(III)TFP(Cl) lead to degenerate set of LUMO orbitals of E symmetry and thus fewer Q bands as compared to that observed of free-base TFP [4], which has D_{2h} symmetry. The blueshift of the Soret and Q bands of Pt(II)TFP relative to Mn(III)TFP(Cl) is consistent with previous observations of hypso/hyper spectra of metalloporphyrins [18]. Moreover, the significant absorption in the 300 to 440 nm spectral region of Mn(III)TFP(Cl), which has been observed previously for Mn(III) porphyrins [18,19] and has been ascribed to the mixing of the Soret transition with ligand to metal charge transfer transitions (LMCT) involving porphyrin and metal $d\pi$ charge transfer transitions [20]. We note that while the structure of the high energy profile has been ascribed to different $\pi \rightarrow \pi^*/CT$ mixing, the energy spacing of 1600 cm⁻¹ is also consistent with a progression in the vibrational modes of the Mn(III) porphyrin ring [21].

The splitting of the Soret band (which will be referred to as the "split Soret band" from here on) is attributed to the mixing of the $\pi \to \pi^*(0)$ transitions with other porphyrin \to metal CT transitions as discussed in detail below

3.3. Transient absorption spectroscopy

Transient absorption (TA) spectra for Mn(III)TFP(Cl) in THF under aerobic conditions is shown in Figure 4A. For Mn(III)TFP(Cl), a ground state bleach (GSB) signal was observed at 475 nm which blue shifts due to overlap with the concomitant evolution of an excited state absorption (ESA) whose maximum at late time is 500 nm (Figure 4A). The ESA exhibited biphasic kinetics which evolved with a time constant of 700 fs, followed by a decay to baseline with a time constant of 9.2 ps (Figure S12A). The GSB evolved similarly with a time constant of 600 fs and a subsequent decay to baseline with a time constant of 11.7 ps indicative of a return to the ground electronic state (Figure S12B). The excited state dynamics are summarized in Figure 5. Following

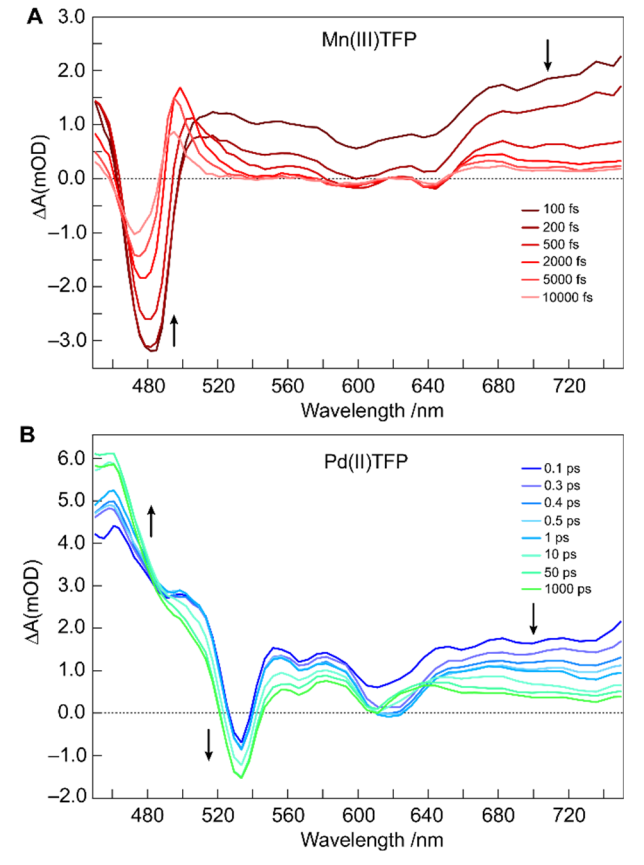


Fig. 4. Transient absorption spectra of **(A)** Mn(III)TFP(CI) and **(B)** Pd(II)TFP in THF at room temperature following photoexcitation at 400 nm.

photoexcitation at 400 nm, the photogenerated singlet excited state (5Sn) of LMCT character relaxes to the singlet excited state (5S1) on a timescale faster than our spectrometer can resolve (<200 fs time constant). As has been identified from magnetic circular dichroism studies of Mn(III)Cl porphyrins [20], the ${}^{5}S_{n}(\pi-\pi^{*})$ LMCT excited states arise from significant mixing of transitions involving porphyrin $\pi \rightarrow \pi^*$ and a multitude of LMCT states involving porphyrin π -orbitals with a minor contribution from the axial chloride. In line with previous assignments [22], the ${}^{5}S_{1}(\pi-\pi^{*})$ excited state decays via intersystem crossing (ISC) to form the ${}^5T_1(\pi$ - π^*) with a resolvable time constant ranging from 600– 700 fs. This state subsequently decays with a time constant of 9-12 ps with a branched kinetic scheme. While most of the decay of the ${}^5T_1(\pi-\pi^*)$ state on that timescale serves to regenerate the electronic ground state, as evidenced by the concomitant decrease in the intensity of the GSB signature, there remains a distinct longer-lived component which persists past 100 ps. Previous reports have assigned this longer-lived state to a ${}^{7}T_{1}(\pi-\pi^{*})$, which decays with a time constant of 80– 140 ps to reform the ground state [22,23]. We note that the conventional dd ligand field states of Mn(III) are heavily mixed with porphyrin and chloride LMCT states,

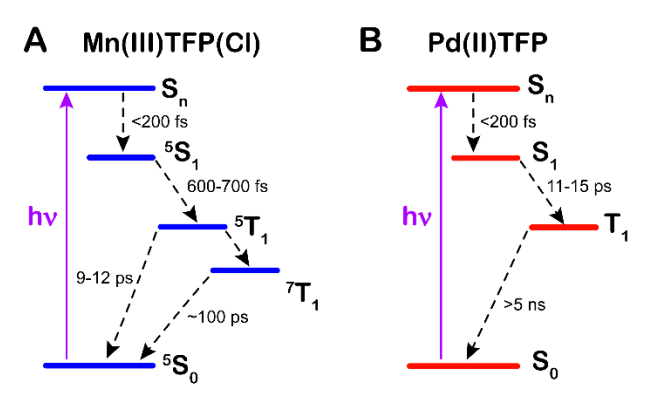


Fig. 5. Jablonski diagram summarizing the excited state dynamics of **(A)** Mn(III)TFP(CI) and **(B)** Pd(II)TFP porphyrins following photoexcitation with 400 nm pump pulses in THF. Dashed lines indicate nonradiative transitions between electronic states that dominate the observed decay kinetics. The singlet and triplet states of the Pd(II) porphyrin are that of Gouterman four-state model. Conversely, for the Mn(III)TFP(CI), the single and triplet ligand field states are heavily mixed with LMCT states of porphyrin and chloride parentages [20].

as deduced from TD-DFT calculations [20], which place the lowest energy LMCT transitions at 15000-16500 cm⁻¹ for Cl \rightarrow d π LMCT and at 22,500 28,000 cm⁻¹ for porphyrin $\pi\rightarrow\pi^*$ and Cl LMCT states. Overall, the kinetics reported here add to these previously reported Mn(III) porphyrin excited state decay kinetics [23] with the inclusion of the sub-picosecond decay ISC dynamics, which heretofore had not been observed.

The TA spectrum for Pd(II)TFP in THF under aerobic conditions exhibits two prominent GSB signatures, at 530 nm and 620 nm, as well as two ESA signatures, one sharp feature at 460 nm and another broad band ranging from 540-750 nm interpenetrated by the GSB at 620 nm (Figure 4B). The prominent ESA feature of Pd(II)TFP, across the 515 -710 nm spectral window decays with a time constant of 11–15 ps (Figure S13) associated with ISC from the S_1 to T_1 . The resultant triplet excited state is captured at longer times and is observed to decay biphasically with lifetimes of 12 and 111 us (Figure S14). These data are consistent with previous reports [24] of ISC from the singlet to the triplet excited state manifold in Pd(II) porphyrins with a time constant on the order of 10 ps with subsequent triplet lifetimes on the hundreds of nanosecond to microsecond timescale.

4. Conclusion

The lifetimes of the metalloporphyrin TFP series is summarized in Table S2. The open-shell, high-spin Mn(III) ion in the tetragonal ligand field imposed by the porphyrin macrocycle leads to a 5S_0 ground state and corresponding 5S_1 excited state in addition to the triplet multiplet manifold of states (5T_1 , 7T_1). This manifold of formal dd states are heavily mixed with the π - π * porphyrinic states [20], opening efficient non-radiative

decay pathways to the ground state [25], thus accounting for the exceptionally short excited state lifetime of both the singlet and the subsequent triplet excited states, as reflected by the immediate decay of the excited state singlet TA signal and the rapid decay of the Mn(III)TFP(Cl) GSB signal in Figure 4. Conversely, these low lying open-shell multiplet states are absent in closed-shell configuration of the Pd(II). Additionally, owing to its strong ligand field d8 configuration, the unoccupied d_{x2-y2} orbital is above that of the porphyrin frontier orbitals, and thus the dd states are inaccessible and do not mediate excited state decay. This is in contrast to the d⁸ configuration of Ni(II)TMP. which is also closed shell but has a weaker ligand field, and consequently there is manifestation of dd states to excited state decay, thus accounting for a triplet lifetime of about 200 ps [26] for Ni(II)TMP as compared to the hundred microsecond lifetime reported here for Pd(II)TFP. Notwithstanding, the decay rate of the Pd(II)TFP(Cl) S₁ state is significantly faster than that of Zn(II)TFP ($\tau = 2.4$ ns [4]) which has a ISC quantum yield of 88% [27]. While $S_1 \rightarrow T_1$ deactivation is the dominant pathway in both Zn(II)TFP and Pd(II)TFP, it is a much more rapid and efficient process in Pd(II)TFP owing to its faster ISC rate. This difference between the Zn(II) and Pd(II) TFP singlet excited state lifetimes is a manifestation of heavy metal-induced spin-orbit coupling which leads to faster ISC of the Pd(II)TFP singlet to its corresponding triplet manifold. In summary, the homologous TFP series of Mn(III), Pd(II) and Zn(II) porphyrins succinctly demonstrate the role of low-lying excited states and spin-orbit coupling on the excited state dynamics of metalloporphyrins.

Authorship contribution statement

[†] As lead authors, WC and SAFA contributed equally. WC and SAFA executed synthesis and characterization.

References

- M. J. Gouterman, Study of the effects of substitution on the absorption spectra of porphin. J. Chem. Phys. 30 (1959) 1139– 1161.
- [2] M. J. Gouterman, Spectra of porphyrins. J. Mol. Spectrosc. 6 (1961) 138–163.
- [3] M. Gouterman, L. C. Snyder, G. H. Wagnière, Spectra of porphyrins. Part II. Four orbital model. J. Mol. Spectrosc. 11 (1963) 108–127.
- [4] P. Chou, L. Kim, S. M. Marzouk, R. Sun, A. C. Hartnett, D. K. Dogutan, S.-L. Zheng, D. G. Nocera, Synthesis, characterization, and hydrogen evolution activity of metallo-meso-(4-fluoro-2,6-dimethylphenyl)porphyrin derivatives, ACS Omega 7 (2022) 8988–8994.
- [5] R. W. Wagner, D. S. Lawrence, J. S. Lindsey, An improved synthesis of tetramesitylporphyrin. Tet. Lett. 27 (1987) 3069–3070.
- [6] G. M. Sheldrick, CELL NOW V2008/2; Bruker AXS Inc; Bruker AXS Inc, 2008.
- [7] SAINT and APEX 2 Software for CCD Diffractometers (Bruker Analytical X-ray Systems, Inc., 2000), Bruker Analytical X-ray Systems, Inc.

BMC, DRM, DKD and DGN contributed to the design, execution and data interpretation of all experiments. MCIG and SLZ performed X-ray crystal data collection and analysis. KGR and BK executed time-resolved experiments. All authors contributed to the writing of the manuscript.

Declaration of competing interest

The authors declare that they have no competing financial interests.

Acknowledgements

M.I.G. acknowledges the Arnold and Mabel Beckman Foundation for an Arnold O. Beckman Postdoctoral Fellowship. DGN acknowledges support provided by grant NSF CHE-1855531. DKD acknowledges Harvard University, Department of Chemistry and Chemical Biology. Use of the Advanced Photon Source, an Office of Science User Facility operated for the U.S. Department of Energy (DOE) Office of Science by Argonne National Laboratory, was supported by the DOE under Contract No. DE-ACO2-06CH11357.

Appendix A. Supplementary material

Supplementary data to this article can be found online. Metrical data for the solid-state structures are available from the Cambridge Crystallographic Data Centre under reference numbers CCDC 2177380 and 2177381 contain the supplementary crystallographic data for this paper. These data can be obtained free of charge via www.ccdc.cam.ac.uk/data_request/cif, or by emailing data_request@ccdc.cam.ac.uk, or by contacting The Cambridge Crystallographic Data Centre, 12 Union Road, Cambridge CB2 1EZ, UK; fax: +44 1223 336033.

- [8] G. M. Sheldrick, TWINABS, Bruker Analytical X-ray Systems, 2014.
- [9] G. M. Sheldrick, SADABS (Bruker Analytical X-ray Systems, Inc., 2014), Bruker Analytical X-ray Systems, Inc.
- [10] G. M. Sheldrick, SHELXT integrated space-group and crystalstructure determination. Acta Cryst. A71 (2015) 3–8.
- [11] G. M. Sheldrick, SHELXL (University of Göttingen, Germany, 2014), University of Göttingen, Germany.
- [12] O. V. Dolomanov, L. J. Bourhis, R. J. Gildea, J. A. K. Howard, H. Puschmann, OLEX2: A complete structure solution, refinement and analysis program. J. Appl. Cryst. 42 (2009) 339–341.
- [13] A. L. Spek, Single-crystal structure validation with the program PLATON. J. Appl. Cryst. 36 (2002) 7–13.
- [14] A. L. Spek, PLATON SQUEEZE: A tool for the calculation of the disordered solvent contribution to the calculated structure factors. Acta Crystallogr. Sect. C Struct. Chem. 71 (2015) 9–18.
- [15] T. R. Ramadhar, S.-L. Zheng, Y.-S. Chen, J. Clardy, Analysis of rapidly synthesized guest-filled porous complexes with synchrotron radiation: Practical guidelines for the crystalline sponge method. Acta Cryst. Section A 71 (2015) 46–58.
- [16] A. J. Rieth, M. I. Gonzalez, B. Kudisch, M. Nava, D. G. Nocera, How radical are 'radical' photocatalysts? A closed-shell

- Meisenheimer complex is identified as a super-reducing photoreagent. J. Am. Chem. Soc. $143\ (2021)\ 14352-14359.$
- [17] C. R. Groom, I. J. Bruno, M. P. Lightfoot, S. C. Ward, The Cambridge Structural Database. Acta. Cryst. B72 (2016) 171– 179.
- [18] K. S. Suslick, R. A. Watson, The photochemistry of chromium, manganese, and iron porphyrin complexes. New J. Chem. 16 (1992) 633–642.
- [19] Y. Fang, L. Wang, W. Xu, Z. Ou, M. Chen. L. Cong, W. Shan, X. Ke, K. M. Kadish, Spectral, Electrochemical, and ESR Characterization of manganese tetraarylporphyrins containing four β , β '-pyrrole fused butano and benzo groups in nonaqueous media. Inorg. Chem. 58 (2019) 2576–2587.
- [20] M. G. I. Galinato, E. P. Brocious, F. Paulat, S. Martin, J. Skodack, J. B. Harland, N. Lehnert, Elucidating the electronic structure of high-spin [Mn^{III}(TPP)CI] using magnetic circular dichroism spectroscopy. Inorg. Chem. 59 (2020) 2144–2162.
- [21] F. Paulat, V. K. K. Praneeth, C. Näther, N. Lehnert, Quantum chemistry-based analysis of the vibrational spectra of fivecoordinate metalloporphyrins [M(TPP)Cl], Inorg. Chem. 45 (2006) 2835–2856.
- [22] Y. Kim, J. R. Choi, M. Yoon, A. Furube, T. Asahi, H. Masuhara, Excited-state dynamics of 5,10,15,20-tetraphenyl-21H,23Hporphine manganese(III) chloride encapsulated in TiMCM-41

- and MCM-41; Proved by fs-diffuse reflectance laser photolysis. J. Phys. Chem. B. 105 (2001) 8513–8518.
- [23] X. Yan, C. Kirmaier, D. A. Holten, Picosecond study of rapid multistep radiationless decay in manganese(III) porphyrins. Inorg. Chem. 25 (1986) 4774–4777.
- [24] C. O. Obondi, G. N. Lim, F. D'Souza, Triplet-triplet excitation transfer in palladium porphyrin-fullerene and platinum porphyrin-fullerene dyads. J. Phys. Chem. C 119 (2015) 119 176–185.
- [25] M.-H. Ha-Thi, N. Shafizadeh, L. Poisson, B. Soep, An efficient indirect mechanism for the ultrafast intersystem crossing in copper porphyrins, J. Phys. Chem. A 117 (2013) 8111–8118.
- [26] V. Balzani, G. Bergamini, S. Campagna, F. Puntoriero, Photochemistry and photophysics of coordination compounds: Overview and general concepts. Top. Curr. Chem. 280 (2007) 1– 36.
- [27] N. C. M. Magdaong, M. Taniguchi, J. R. Diers, D. M. Niedzwiedzki, C. Kirmaier, J. S. Lindsey, D. F. Bocian, D. Holten, Photophysical properties and electronic structure of zinc(II) porphyrins bearing 0–4 meso-phenyl substituents: Zinc porphine to zinc tetraphenylporphyrin (ZnTPP). J. Phys. Chem. A. 124 (2020) 7776–7794.